Change of the band structure and electronic phase transitions in Bi and $Bi_{1-x}Sb_x$ alloys under uniaxial tension strains

N. B. Brandt, V. A. Kul'bachinskiĭ, N. Ya. Minina, and V. D. Shirokikh

Moscow State University

A procedure is developed for the production of strong ($\sim$ 0.5%) reversible strains in bulky single crystals. The procedure is based on deformation of a complicated system of which the sample is a part. The strain in such a system is calculated and it is shown that in the central part of the sample it is uniform and of the uniaxial tension type. The ratio of the diagonal components of the strain tensor can vary, depending on the geometry of the system and on its elastic moduli. The procedure was used to investigate the Shubnikov–de Haas effect in Bi, as well as in semimetallic and semiconducting $Bi_{1-x}Sb_x$ alloys in tension along the binary and bisector axes. The change of the Fermi surface is investigated, and the McClure theory is used to calculate the character of the displacement of the terms in the L and T points under deformation. It is shown that in the entire deformation region the change of the anisotropy and of the orientation of the hole ellipsoid and of the electron "ellipsoids" does not exceed 10–15%. Also observed and investigated are the I. M. Lifshitz electronic phase transitions connected with the following topological changes of the Fermi surface: $3e + 1h \rightarrow 2e + 1h$; $3e \rightarrow 1e$; $3e \rightarrow 2e$; semiconductor$\rightarrow$semimetal with ellipsoids $1e + 1h$ and $2e + 1h$. A pseudopotential method using 160 plane spinor waves is used to calculate the change of the energy spectrum of the Bi in deformations of the indicated type. The results of the calculation agree well with the experimental data.

PACS numbers: 64.70.Kb, 46.30.Lx, 46.30.Rc, 71.25.Rk

INTRODUCTION

Investigations of the dependence of the parameters and structure of the spectrum on the parameters of the crystal lattice reveals not only the possibility of practical applications, but also additional possibilities of verifying various theoretical models on which both numerical calculation methods of the band structure and model representations of the spectrum are based. Most studies in this field (see, e.g., the reviews[1-3]) are devoted to the investigation of the influence of hydrostatic compression on the Fermi surface (FS) of metals.

Further developments in this direction are the studies of the physical properties of substances under uniaxial compression or tension. The most interesting feature of uniaxial strains is the possibility of changing the symmetry of the crystal lattice; this distinguishes them in principle from hydrostatic compression and can lead, even at small strains, to qualitative changes in the spectrum. The high-sensitivity of the electric, magnetic, and other characteristics to uniaxial deformations and the ensuing possibility of obtaining substances with new properties make research in this field most interesting.

Studies under uniaxial deformations have by now been made on many simple metals, such as white tin,[4,5] lead,[6] indium, and aluminum.[7] Also investigated were noble[8,9] and some transition metals.[10] However, because of the low elastic limits of most metals (100–300 kgf/cm²), the attained strains $\varepsilon \sim 10^{-2}\%$ and the observable effects are quite small. Much larger uniaxial strains can be obtained in a number of semiconductors (Ge, Si) and semiconducting compounds (InSb, HgSe), owing to the higher elastic limit (up to 2×10^4 kgf/cm², Ref. 11). As a result, this class of substances was better investigated under uniaxial deformations than the metals.

It should be noted that elastic extension up to 1–2% can be produced in whisker crystals. However, the inconvenience of working with such small objects, the arbitrary crystallographic orientation of their growth, and the difficulty of obtaining whiskers of many elements, alloys, and compounds makes it urgent to seek for new methods of producing strong elastic strains in bulky crystals.

Methods have been recently developed, whose main idea is either to produce lateral support of the deformed sample by the matrix in which the compression is effected,[12] or by deforming a complex system of which this sample is a part.[13] The most successful modification of these methods, which makes possible reversible strains $\varepsilon \sim 0.5\%$ of the uniaxial tension or compression type with high degree of homogeneity in the investigated part of the sample, is the procedure developed and employed in the present study.

This procedure was used to investigate the Shubnikov–de Haas (SdH) effect in bulky single crystals of Bi and $Bi_{1-x}Sb_x$ alloys in tension along the binary and bisector axes up to strains 0.5%, to obtain detailed information on the change of the Fermi surface, and to observe a number of I. Lifshitz's topological electronic transitions.[14] The pseudopotential method is used to calculate the change of the band structure of Bi under uniaxial deformations of the investigated type, and the experimental and calculated relations are compared.

STRAIN-PRODUCTION PROCEDURE

To increase the elastic (or reversible) strain, we used the idea of producing on the surface of the sample boundary conditions such that, on the one hand, maxi-
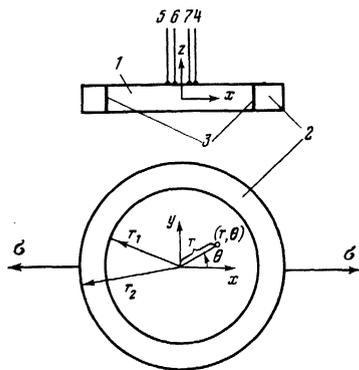
0038-5646/80/030562-10$02.40
© 1980 American Institute of Physics 562

FIG. 1. Sample in ring: 1—sample, 2—ring, 3—gap filled with Araldit resin, 4,5—current contacts, 6,7—potential contacts.

mum possible strains are produced, and on the other, damage to the sample is prevented. To realize this idea, the sample in the form of a disk is rigidly mounted in a ring having a Young's modulus much larger than that of the sample, in such a way that the gap, between the sample and the ring, filled with Aral'dit resin, is negligibly small compared with the sample dimensions (Fig. 1).

It follows from general considerations that the character of the strain produced in the sample when the ring is under tension should differ from the strain due to the uniaxial stretching of a free sample. It is also obvious that the deformation of the sample as a whole is not uniform. Therefore the possibility and benefits of using such a procedure are determined, first, by the dimensions of the region where the strain of the sample is sufficiently uniform, second, by the value of this strain, and third, by the possibility of measuring effects connected only with the uniformly deformed region of the sample.

To solve these problems we calculated the strains produced in the system when stretched by two concentrated forces. Since the sample is a disk, a planar stressed state is produced in the sample and in the ring. To describe this state we used the stress function $\varphi(r, \theta)$ proposed by Papkovich,[15] in the form

$$\varphi_1(r, \theta) = B_0^{(1)} r^2 + \sum_{k=2,4,6,\ldots} (A_k^{(1)} r^k + C_k^{(1)} r^{k+2}) \cos(k\theta), \tag{1}$$

$$0 \leqslant r \leqslant r_1, \quad 0 \leqslant \theta \leqslant 2\pi$$

for the disk and in the form

$$\varphi_2(r, \theta) = B_0^{(2)} r^2 + C_0^{(2)} \ln r + \sum_{k=2,4,6,\ldots} (A_k^{(2)} r^k + B_k^{(2)} r^{-k} + C_k^{(2)} r^{k+2} + D_k^{(2)} r^{-k+2}) \cos(k\theta),$$

$$r_1 \leqslant r \leqslant r_2, \quad 0 \leqslant \theta \leqslant 2\pi \tag{2}$$

for the ring.

Here r and θ are the polar coordinates of the variable point of the ring or disk, θ is the angle reckoned from the direction of the applied force σ, as shown in Fig. 1, r_1 is the radius of the disk, and r_2 is the outer radius of the ring. The quantities $B_0^{(1)}$, $A_k^{(1)}$, $C_k^{(1)}$, $B_0^{(2)}$, $C_0^{(2)}$, $A_k^{(2)}$, $B_k^{(2)}$, $C_k^{(2)}$, and $D_k^{(2)}$ are indeterminate coefficients.

Since the stress function determines the stress ten-

sor, which is connected by Hooke's law with the strain tensor, the solution of the problem of the planar stressed state of the strained body reduces thus to determining the indeterminate coefficients of the series (1) and (2). We used for this purpose the boundary conditions on the outer periphery of the ring and the conditions for joining-up the solutions for the disk with the solution for the ring on its inner periphery. Since the sought stress functions are series in powers of r, the components of the stress tensor, as well as the displacement vector δr of any point, are also represented in the form of series in powers of r. The joining-up condition and the boundary conditions are satisfied by equating, term by term, the series solutions for the ring with the series solutions for the disk. This calculation procedure determines the strain tensor components ε_{xx}, ε_{yy}, ε_{zz}, ε_{xy} and the stress tensor components σ_{xx}, σ_{yy}, σ_{zz}, σ_{xy} for any point (x, y) of the sample in the rectangular coordinate system shown in Fig. 1.

The actual calculation of the strain was carried out for Bi samples whose trigonal axis was perpendicular to the plane of the ring. In this case the Young's modulus E_1 and the Poisson coefficient ν_1 corresponding to tension and compression in the basal plane of the crystal are 3.88×10^{11} dyne/cm^2 and 0.31, respectively, while the Poisson coefficient ν_0 that determines the change of the sample dimensions along the trigonal axis is 0.43.[16] The Young's modulus of the ring is $E_2 = 20 \times 10^{11}$ dyne/cm^2, and its Poisson coefficient is $\nu_2 = 0.33$ (40 KhNYu heat-treated steel). The calculations were performed with a computer for a tension force 15 kgf. The average values of the strains $\bar{\varepsilon}_{xx}, \bar{\varepsilon}_{yy}, \bar{\varepsilon}_{zz}$ in the central part of the sample, of radius $r_0 = 0.15 r_2$, and of their inhomogeneities $\eta_{xx}, \eta_{yy}, \eta_{zz}$ in this region, at $r_2 = 2$ mm and at a ring and sample thickness 0.8 mm are listed in Table I. The subsequent measurements were made at $r_1/r_2 = 0.75$.

Figure 2 shows the strain-tensor components $\varepsilon_{xx}(r, \theta)$, $\varepsilon_{yy}(r, \theta)$, $\varepsilon_{zz}(r, \theta)$ along the radius of the sample at various values of the angle θ and at $r_1/r_2 = 0.75$. When the force is applied to the ring, the sample is stretched along the applied force and compressed in a perpendicular direction. The quantities ε_{xx} and ε_{yy} are maximal at the center and are decreasing functions of the distance from the point to the center of the sample, with the exception of a small region of angles θ near the x axis. As seen from Fig. 2, ε_{xx} and ε_{yy} are practically constant in the region $r < 0.2 r_1$, while ε_{xy} is negligibly small in this region. The component ε_{zz} is several times smaller than ε_{xx} and ε_{yy}, and its mean value does not depend on the averaging area. Calculation yields the following values of the strain at the

TABLE I.

r_1/r_2	$\bar{\varepsilon}_{xx} \cdot 10^3$	$\bar{\varepsilon}_{yy} \cdot 10^3$	$\bar{\varepsilon}_{zz} \cdot 10^3$	η_{xx}, %	η_{yy}, %	η_{zz}, %
0.3	1.26	−0.7	−0.32	1.53	1.68	1.40
0.4	1.36	−0.84	−0.34	1.43	1.39	1.64
0.5	1.57	−1.02	−0.36	1.37	1.19	1.92
0.6	1.82	−1.22	−0.38	1.37	1.11	2.16
0.7	2.04	−1.40	−0.42	1.46	1.20	2.25
0.75	2.13	−1.45	−0.44	1.55	1.32	2.22
0.8	2.2	−1.47	−0.47	1.65	1.49	2.13
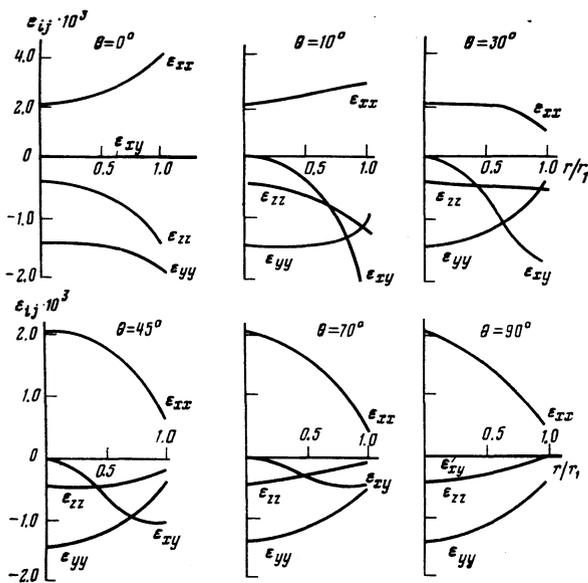
FIG. 2. Variation of the strain-tensor components ε_{xx}, ε_{yy}, ε_{zz}, ε_{xy} along the sample radius (θ is the angle between the direction of the radius and the x axis), $\sigma = 15$ kgf.

central part of the sample:

$$\varepsilon_{xx} = 0.014\% \text{ kgf}^{-1}, \quad \varepsilon_{yy} = -0.01\% \text{ kgf}^{-1}, \quad \varepsilon_{zz} = -0.002\% \text{ kgf}^{-1}.$$

An increase of Young's modulus of the ring decreases the strain more the larger the ring. For rings with $r_1/r_2 \geq 0.75$ the value of ε_{yy} ceases to depend on the ratio E_2/E_1, whereas ε_{xx} continues to change noticeably. This leads to an interesting property of the system: at $r_1/r_2 \geq 0.75$ the change of Young's modulus of the ring makes it possible, at a given load, to separate the effect of pure uniaxial tension, wherein the sample dimensions change only along the action of the force.

In the actual application of the described deformation method, the sample and the ring of 40KhNYu material, with "lugs" for stretching, were cut in accordance with special programs with a program-controlled electric-spark lathe in such a way that the gap between them, filled with polymerized Aral'dit resin, did not exceed 15–20 μm. The trigonal axis of the sample C_3 was perpendicular to the plane of the ring, while the binary axis C_2 and the bisector axis coincided with the tension direction. Since the experimental determination of the strain in the central part of the sample entails great difficulties, and attempts to measure them with an FKPA-1 strain pickup or with silicon whisker crystals yielded values that differed by 40%, we use henceforth the calculated strain values presented above. The resultant error can be due only to the nonlinearity of $\varepsilon(\sigma)$, which can be produced in the system by plastic deformation on the boundary of the sample and the ring. However, the fact that glide bands appear on the peripheral sections of the sample after etching only at $\sigma \gtrsim 25$ kgf allows us to assume that the nonlinearity of $\varepsilon(\sigma)$ in the central region, if it does take place, is small for most employed loads.

Current and potential electrodes of copper wire 30 μm in diameter were soldered to the sample by the electric-spark method along the direction of application of the force (see Fig. 1) in such a way that the distance between the potential contacts, which were located in the central uniformly deformed region, did not exceed 0.5–0.6 mm. It is obvious that the locations of the current lines in the system shown in Fig. 1 are such that the contribution to the oscillatory dependence of the magnetoresistance is determined only by the central uniformly deformed part of the sample, whereas substantially non-uniformly deformed peripheral regions of the sample can contribute only to the monotonic dependence of the resistance on the magnetic field. It is also obvious that to separate the oscillating signal from the central region, the current contacts are best placed as close as possible to the potential contacts.

The oscillations of the magnetoresistance were recorded by a standard procedure with the direct current modulated at a frequency 22 Hz. To separate frequencies with different angular dependences relative to the crystallographic axes we used both longitudinal and transverse modulation of the magnetic field. Magnetic fields up to 50 kOe were produced in superconducting magnetic systems.

CHANGE OF ENERGY SPECTRUM OF Bi AND $Bi_{0.995}Sb_{0.005}$ UNDER TENSION

The influence of uniaxial strains on the energy spectrum of Bi has not been systematically investigated so far. The presently available information, obtained by studying the galvanomagnetic characteristics,[17] the thermomagnetic coefficients,[18] and oscillation effects[9] pertain mainly to uniaxial compression up to a strain $\sim 10^{-2}\%$ along the trigonal axis of the crystal. Under these conditions the change of the energy spectrum of Bi is similar to its change under hydrostatic compression. Some information on the change of the Fermi surface of Bi deformed along other crystallographic directions were obtained from magnetorestriction measurements,[20] and using whiskers under tension.[21] The change of the Fermi surface of bismuth compressed along the principal crystallographic directions was investigated by us earlier[22] with the aid of the SdH effect at strains 0.4–0.5%.

In the present study tension was produced in the Bi samples along the binary and bisector axes by the procedure described above at loads up to $\sigma = 30$ kgf and liquid-helium temperature. The high homogeneity of the strain in the investigated part of the sample made it possible to observe, with the aid of the SdH effect, the changes produced by application of the load in all the sections from which oscillations are usually observed at $\sigma = 0$. For convenience in the determination of any of the components of the strain tensor, all the results are presented as functions of the load.

At $\sigma \| C_2$ the SdH oscillations were investigated with the magnetic field intensity vector H rotating in the trigonal–bisector[1] plane and at $H \| C_2$.[23] At $\sigma \| C_1$ the ShD were investigated in the $(C_2 C_3)$ plane, as well as at $H \| C_1$. The frequencies were separated by using longitudinal and transverse modulation of the magnetic field, Fourier analysis with a computer was used. In the most complicated cases, the Fermi surface sections
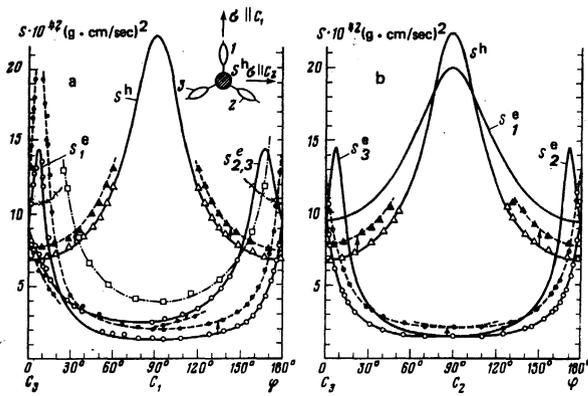
564   Sov. Phys. JETP 51(3), March 1980

Brandt *et al.*   564

FIG. 3. Angular dependences of the extremal sections of the Fermi surface of bismuth: a—in the plane $(C_1C_3)(\sigma\|C_2)$, b—in the plane $(C_2C_3)(\sigma\|C_1)$. Loads σ, kgf: a—0(o,△),8(●,▲), 29(□,*); b—0(o,△),9(●,▲). Solid, dashed, and dash-dot lines are drawn in accordance with the ellipsoidal model.

FIG. 4. Plots of the relative change of the cross sections $\Delta S/S$ of the Fermi surface of bismuth against the load: a—at $\sigma\|C_2$, b—$\sigma\|C_1$. The measurements were made in the interval of angles φ between H and C_1: a) □,■—90°< φ < 110°, H$\|C_2$; △,▲— 0< φ < 50°,130°< φ < 180°; o,●—20°< φ < 160°; ◇,◆—0< φ < 180°; b) □,■—H$\|C_1$; △,▲—0< φ < 50°; o—H$\|C_1$; ◇—0< φ < 90°; ◆—90° < φ < 180°. The light and dark symbols pertain to different samples, the solid and dash-dot lines pertain to calculation of the change of the sections by the McClure model, and the dashed lines pertain to calculation by the pseudopotential method. The dotted curve shows the change of the concentration of the electrons in the "ellipsoid" 1 at $\sigma\|C_1$.

were determined accurate to 2-3%, and only for directions at which the change of the position of the Fermi level in the magnetic field becomes noticeable (the maximal electron and hole sections) did the error in the cross sections increase to 10-15%. The angular dependences of the Fermi-surface sections of Bi in the (C_1C_3) and (C_2C_3) plane and their change under tension are shown in Figs. 3a and 3b (the schematic arrangement of the equal-energy surfaces of Bi relative to the crystallographic axes is shown in the upper part of the figure).

In contrast to hydrostatic compression and compression along the C_3 axis, when all three electron equal-energy surfaces decrease to the same degree, in the case of tension along the axes C_2 and C_1 a qualitatively different change is observed in Bi for the volumes of the electron "ellipsoids" that are differently oriented relative to the tension direction. At $\sigma\|C_2$ the sections S_1^e and S^h increase, whereas the sections $S_{2,3}^e$ decrease. At $\sigma\|C_1$, the character of the change of the electron "ellipsoids" is reversed: $S_{2,3}^e$ increase while S_1^e decreases. The hole ellipsoid increases in both cases. The relative variation of the Fermi-surface sections with load are shown in Fig. 4 for two Bi samples. The illustrated plots of $\Delta S/S$ against σ describe the change of the Fermi surface at all the investigated orientations (see Fig. 3) for 10 samples. The initial rates of change of the sections are given in Table II. It must be noted that the largest change in the frequency of the oscillations when the crystal is deformed is accompanied only by a weak decrease of their amplitude, and good reversibility of the results is observed when the load is removed.

The C_1^e sections of the "ellipsoid" that increased in tension along the C_2 axis were measured at σ =8 kgf ($\varepsilon_{xx} \approx 0.11\%$) in an angle interval of practically 180°, and at σ =29 kgf ($\varepsilon_{xx} \approx 0.41\%$) in the interval 20° < φ < 160°. Within the limits of the indicated accuracy with which the sections were determined, no change was observed in the anisotropy of this "ellipsoid" when the crystal was deformed. Similarly, all the observed hole sections and sections of the "ellipsoids" 2 and 3 at
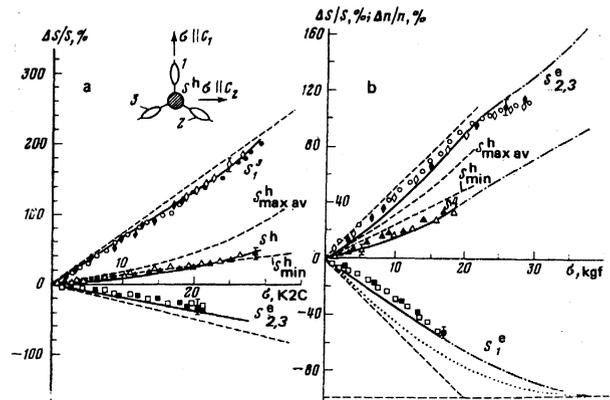
$\sigma\|C_1$ change by the same percentage, corresponding to the data of Fig. 4. An investigation of the anisotropy of the decreasing electron "ellipsoid" in both orientations is made difficult by the rapid decrease of the amplitude of the corresponding oscillations.

The angle of inclination of the electron "ellipsoids" to the basal plane is characterized by the angle distance between their midsection and the previous direction of the C_3 axis—see Fig. 3a. According to the angular dependences of the sections of the Fermi surface in the trigonal–bisector plane, which are shown in this figure, the angle of inclination of ellipsoid 1 at $\sigma\|C_2$ remains constant accurate to ~1° up to $\sigma \approx 8$ kgf, and with accuracy ~10° up to $\sigma \approx 30$ kgf. There is likewise no noticeable change of the angles of inclination of the growing "ellipsoids" 2 and 3 at $\sigma\|C_1$ (Fig. 3b).

Thus, a strong anisotropic deformation of the crystal lattice leads to a strong change in the volume of the remaining parts of the FS, without producing a noticeable change in the anisotropy and in the inclination angles, at least in the case of the growing electron ellipsoids.

The cyclotron effective masses were determined at $\sigma\|C_2$ for the directions H$\|C_1$ and H$\|C_3$ from the temperature dependence of the oscillations of the magnetoresistance up to loads σ =10 kgf. In the former case the effective mass corresponds to the near-minimal section of the growing electron "ellipsoid" 1, and in the second

TABLE II.

	$\partial \ln S/\partial\sigma$, %/kgf	
	$\sigma\|C_2$	$\sigma\|C_1$
$\partial \ln S_1 e/\partial\sigma$	6.4±0.3	−3.0±0.3
$\partial \ln S_{2,3}{}^e/\partial\sigma$	−1.8±0.2	4.4±0.3
$\partial \ln Sh/\partial\sigma$	1.4±0.2	1.8±0.2

to the minimal section of the hole ellipsoid. The minimal cyclotron mass of the electrons m_c^e increases under tension to 150% at $\sigma = 10$ kgf, and the minimal cyclotron mass of the holes at the point T of momentum space remains unchanged, with accuracy 10%, in the investigated load region.

Since strains ~0.5% are still much too small to lead to a noticeable change of the parameters of the McClure model[24] of the energy spectrum, this model was used to estimate the motion of the terms at the points L and T under tension. The spectrum of the hole at T is assumed quadratic in first-order approximation.

McClure's dispersion law is of the form

$$(\varepsilon - \tfrac{1}{2}\varepsilon_{gL} - \tfrac{1}{2}\alpha_c k_y{}^2)(\varepsilon + \tfrac{1}{2}\varepsilon_{gL} + \tfrac{1}{2}\alpha_v k_y{}^2) = Q_{11}{}^2 k_x{}^2 + Q_{22}{}^2 k_y{}^2 + Q_{33}{}^2 k_z{}^2, \quad (3)$$

where ε_{gL} is the energy gap at the point L, ε is the energy reckoned from the center of the energy gap at L; the principal directions of the Fermi surface are $k_x \| C_2$, k_y in the elongation direction of the ellipsoid, and k_z perpendicular to k_x and k_y. The parameters of the bismuth spectrum are chosen to be $Q_{11} = 0.465$, $Q_{22} = 0.0333$, $Q_{33} = 0.346$, $\alpha_c = 0.80$; $\alpha_v = 1.19$ (in atomic units) and $\varepsilon_{gL} = -9$ meV.[25] The changes of ε_F and of the sections of the Fermi surface under deformation were calculated under the assumption that the terms move linearly at the points L and T with the strain, that the volumes of the hole and electron ellipsoids are equal, and that ε_{gL} remains unchanged. It should be noted that at $\varepsilon_F \gg \varepsilon_{gL}$ the change of ε_{gL} within the framework of the spectrum (3) has a most negligible effect on the sizes of the Fermi-surface sections.

A computer was used to select ε_F at each extremum to make the ellipsoid sections that correspond to the model (3) agree best with the experimental data. The scheme of the motion of the energy bands of bismuth near the Fermi level in the course of stretching is shown in Fig. 5, and the change of the extremal sections of the Fermi surface corresponding to this motion and calculated in accord with the model (3) is shown by the solid lines of Fig. 4.

We note that some discrepancy between the experimental and calculated data on Fig. 4 cannot be attributed to a possible nonlinearity of the dependence of the strain on the load σ, since allowance for this non-linearity, while improving the agreement between the experimental and calculated data for certain curves, makes this agreement simultaneously worse for others.

We investigated also the influence of tension along the axes C_1 and C_2 on the Fermi surface of the alloy $Bi_{0.995}Sb_{0.005}$. It is known that in $Bi_{1-x}Sb_x$ alloys a smoother transition takes place with increasing x, from the energy spectrum of Bi to the spectrum of Sb, with formation of a semiconducting phase in the concentration interval $6.5 \lesssim x \lesssim 22$ at.%. The energy spectrum of the investigated semimetallic alloy $Bi_{0.995}Sb_{0.005}$ differs from the spectrum of pure Bi only by a somewhat smaller overlap of the extrema at L and T. It was observed that the change of the spectrum of the alloy $Bi_{0.995}Sb_{0.005}$ is similar to that observed for pure Bi: the plots of $\Delta S/S$ against σ for the electrons and holes coincide fully with those shown in Fig. 4b. A distinguishing feature of this alloy is that in fields above 5 kOe the oscillations from the hole ellipsoid dominate in the entire range of angles, so that it is possible to observe both the minimal and the maximal Fermi-surface sections. The anisotropy of the hole surface in the investigated strain region remains unchanged within the accuracy 10–15% at which the maximum hole sections are determined.

THE ELECTRONIC TRANSITIONS OF I. LIFSHITZ

The common character of the displacements of the electron and hole extrema of Bi and of the $Bi_{1-x}Sb_x$ alloys under tension (Fig. 5) shows that at sufficiently large strains one should observe in these substances the entire series of the electronic phase transitions (EPT) of I. Lifshitz.[14] These transitions were first observed under hydrostatic compression in investigations of the baric dependence of the components of the magnetoresistance tensor of doped Bi,[26] of the asymptotic behavior of the magnetoresistance of Cd,[27] and the pressure dependence of the temperature of the superconducting transition of Te and its alloys.[28] Uniaxial deformations, by changing the symmetry of the crystal, greatly extend the possibilities of observing EPT.

In the present studies of Bi, of $Bi_{0.924}Sb_{0.076}Te$ alloys, and of the superconducting alloy $Bi_{0.925}Sb_{0.075}$ in tension along the C_2 and C_1 axes, we investigated EPT of the following types: 1) $3e + 1h \rightarrow 2e + 1h$, 2) $3e \rightarrow 1e$, 3) $3e \rightarrow 2e$, 4) semiconductor $\rightarrow$ semimetal with formation of the ellipsoids $2e + 1h$ and $1e + 1h$ (the letters e and h stand respectively for the electron and hole ellipsoids).

The transition $3e + 1h \rightarrow 2e + 1h$

A transition of this type takes place when bismuth is stretched along the bisector axis. Attention must be called first to the fact that extrapolation of the dependence of $\Delta S_1^e/S_1^e$ on σ of a decreasing ellipsoid (see Fig. 4b) to a value -100% (as was done in Refs. 21 and 29) can lead to an error in the determination of the critical strain corresponding to the transition. The reason is that the character of the change of the sections S_1^e under load depends not only on the dispersion of the carriers, but also on the initial band structure and on the character of the displacement of the other extrema. In the
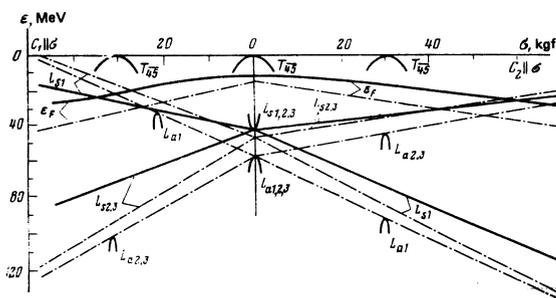

FIG. 5. Motion of electron and hole extrema at the point L and of the Fermi level relative to the top of the valence band at T of bismuth under tension. Solid lines—calculation by McClure's model, dash-dot—calculation by the pseudopotential method.

considered case, the presence of a hole extremum at the point T of Bi, shifting in the same direction as the vanishing extremum L_1, causes the vanishing of the ellipsoids at L_1 to be delayed and the true value of the critical strain can be determined only by calculation. Such a calculation requires not only knowledge of the dispersion law but also data on the terms L_{ai}, L_{si}, T_{45} under deformation, and these data are practically impossible to obtain from experiment.

According to the calculation by the McClure model, under the assumption that the terms move linearly and that the gaps in the spectrum remain unchanged (see Fig. 5 above), the vanishing of the ellipsoid 1 takes place at $\sigma_{cr} \approx 38$ kgf ($\varepsilon_{xx} \approx 0.053\%$, $\varepsilon_{yy} \approx - 0.38\%$, $\varepsilon_{zz} \approx - 0.076\%$). The change in the gap ε_{gL}, which was neglected in the calculation, can lead to another change of the anisotropy of the ellipsoid at L_1 under load, differing from that obtained by assuming a constant ε_{gL}. However, this change cannot shift significantly the obtained value of σ_{cr} and manifests itself principally in the character of the dependence of S on σ. The character of the change of the sections of all the Fermi-surface ellipsoids corresponding to the transition $3e + 1h \rightarrow 2e + 1h$ at $\sigma \| C_1$ is shown in Fig. 4b by dash-dot lines.

In the region of strains preceding the vanishing of the sections S_1^e, the carrier density is so low (dash-dot line in Fig. 4b) that the contribution of the electrons at L_1 to the electric conductivity becomes unobservable. The character of the change of the carrier density in the ellipsoid 1 should lead to irregularities in the change of the volumes of the increasing electron and hole ellipsoids. At $\sigma \| C_1$ this irregularity is observed experimentally on the plot of $\Delta S_{2,3}^e / S_{2,3}^e$ against σ (see Fig. 4b). A characteristic feature of these anomalies is that the inflection region on the plots of $\Delta S/S$ against σ lies to the left of the critical load. A similar shift to the left of the transition point should be observed for the regularities on the plot of the resistance against the load, a fact pointed out by Lifshitz in Ref. 14.

At $\sigma \| C_2$ the transition $3e + 1h \rightarrow 1e + 1h$ should take place at $\sigma_{cr} \approx 56$ kgf ($\varepsilon_{xx} = 0.78\%$, $\varepsilon_{yy} = - 0.56\%$, $\varepsilon_{zz} = - 0.11\%$), a value exceeding the capabilities of the employed strain-production method. Therefore no irregularity preceding the EPT was observed in the plot of $\Delta S_1^e / S_1^e$ against σ for the growing ellipsoid.

The $3e \rightarrow 1e$ transition

An EPT transition of this type is observed for the alloy $Bi_{0.924}Sb_{0.076}Te$ with Te concentration $\approx 10^{-4}$ at.% when stretched along the binary axis.[30] This alloy is a semiconductor with a direct gap $\varepsilon_{gL} \approx 11$ meV and an indirect gap between the extrema at L and T, with value $\varepsilon_g \approx 7$ meV. The Te impurity fills the electron extrema in L. The small value $\varepsilon_F^e \approx 10$ meV makes it possible to observe in this alloy a transition to a single-ellipsoid electron Fermi surface ($\sigma \| C_2$) at smaller strains than in pure Bi. The general character of the change of the Fermi surface of $Bi_{0.924}Sb_{0.076}Te$ under tension agrees fully with that observed for Bi and for the alloy $Bi_{0.995}Sb_{0.005}$.
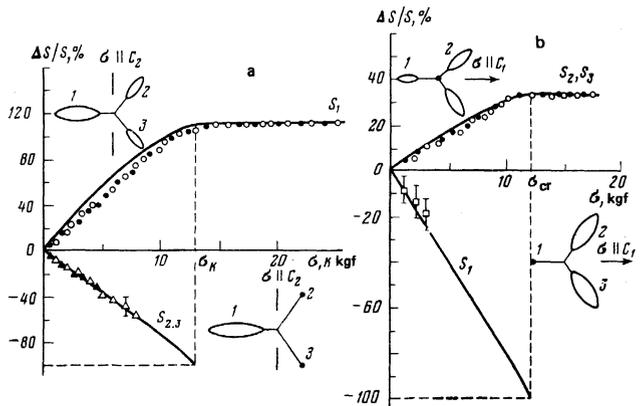

FIG. 6. Plots of the relative change of the Fermi-surface sections of the alloy $Bi_{0.924}Sb_{0.076}Te$ against the load $\sigma \| C_2$ (a) and $\sigma \| C_1$ (b), observed in the interval of angles φ between H and C_3: a) $\circ, \bullet -95° < \varphi < 180°$; $\triangle, \blacktriangle -0 < \varphi < 10°$; b) $\circ, \bullet - 0 < \varphi < 180°$; $\square - H \| C_1$. The light and dark symbols pertain to different samples. Solid lines—calculation by the McClure model.

The relative change of the increasing and decreasing sections S_1 and $S_{2,3}$ with changing load at $\sigma \| C_2$ is shown in Fig. 6a. This dependence is the same for all the observed sections of ellipsoids 1, 2, and 3. The solid lines on Fig. 6a are the result of computer calculation by McClure's model performed just as for pure Bi, except that it is assumed here that the initial concentration is preserved, rather than that the concentrations of the electrons and holes are equal. The parameters for the alloy were taken from Refs. 31 and are (in atomic units): $Q_{11} = 0.412; Q_{22} = 0.016; Q_{33} = 0.329$; $\alpha_c = 0.63$, $\alpha_v = 1.0$; $\varepsilon_{gL} = 10$ meV.

According to the calculation that agrees well with the experimental data, the sections of the "ellipsoids" 2 and 3 vanish at $\sigma_{cr} \approx 13$ kgf ($\varepsilon_{xx} \approx 0.18\%$, $\varepsilon_{yy} \approx - 0.13\%$, $\varepsilon_{zz} \approx - 0.026\%$). It is obvious that at the point σ_{cr} an EPT takes place to a single-ellipsoid electron surface. The stopping of the growth of "ellipsoid" 1 and the approximate threefold increase of its volume at $\sigma > \sigma_{cr}$ indicate that all the carriers go over from $L_{2,3}$ to the extremum L_1 at the EPT point. The rate of divergence of the electronic extrema in the case along C_2 is ≈ 1.3 meV/kgf. The amplitude of the oscillations from the vanishing ellipsoids decreases rapidly against the background of the dominant oscillations from the growing "ellipsoid" 1 (Fig. 7).

The monochromaticity of the SdH oscillations at $\sigma > \sigma_{cr}$ (when one ellipsoid remains in the spectrum) has made it possible to determine with high accuracy the parameters of the single-ellipsoid electron surface, to ascertain that its anisotropy and inclination angle remain unchanged upon deformation, and also to observe for the first time for the $Bi_{1-x}Sb_x$ system in the (C_1C_3) planes two spin-damping angles: $\varphi_{d_1} = 1.5° \pm 0.5°$ and $\varphi_{d_2} = 8° \pm 0.5°$, which do not change in the interval $12 < \sigma < 24$ kgf.

The transition $3e \rightarrow 2e$

When the $Bi_{0.924}Sb_{0.076}Te$ alloy is stretched along the bisector axis, a transition is observed from a three-ellipsoid to a two-ellipsoid electron Fermi surface,[30]
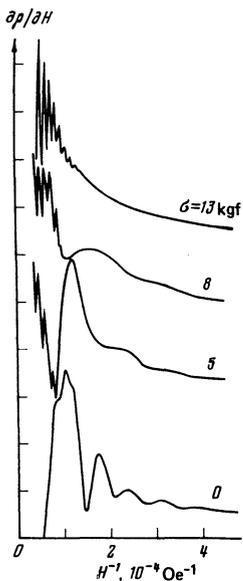
567   Sov. Phys. JETP 51(3), March 1980

Brandt et al.   567

FIG. 7. Plots of $\partial\rho/\partial H$ against H^{-1} for the alloy $Bi_{0.924}Sb_{0.076}Te$ at $\sigma\|C_2$; H in the (C_1C_3) plane is inclined away from the C_3 axis by $5°$. The loads σ (kgf) are marked on the curves.

FIG. 8. Plots of $\partial\rho/\partial H$ against $1/H$ for the alloy $Bi_{0.925}Sb_{0.075}$ at $\sigma\|C_2$ and $H\|C_1$. The loads σ (in kgf) are marked on the curves.

which is accompanied by simultaneous vanishing of one "ellipsoid" and the cessation of the growth of the sections of the two remaining ones (Fig. 6b).

The absence of holes in T in this case causes the character of the plots of S_1 and $S_{2,3}$ against σ near the EPT to differ qualitatively from the analogous plots for pure Bi (see Fig. 4b). The transition takes place at $\sigma_{cr} \approx 12$ kgf ($\varepsilon_{xx} \approx 0.17\%$, $\varepsilon_{yy} \approx -0.12\%$, $\varepsilon_{zz} \approx -0.0024\%$) with complete transfer of the carriers from L_1 to $L_{2,3}$, as indicated by the increase of the value of "ellipsoids" 2 and 3 at $\sigma \gtrsim \sigma_{cr}$ by an approximate factor of 1.5. The rate of divergence of the terms L_1 and $L_{2,3}$ is in this case ≈ 0.9 meV/kgf.

SEMICONDUCTOR–SEMIMETAL TRANSITION

The semiconductor–semimetal EPT was observed in the n-type semiconductor alloy $Bi_{0.925}Sb_{0.075}$, with carrier density $\approx 10^{15}$ cm^{-3}, stretched along the C_2 and C_1 directions. This alloy is characterized by an energy gap ≈ 7 meV between the valence band and the conduction band,[32] and has a semiconductor-type temperature dependence of the resistance. When the samples were stretched along the binary or bisector axes at a certain load $\sigma_{cr} \approx 10$ kgf ($\varepsilon_{xx} \approx 0.14\%$, $\varepsilon_{yy} \approx -0.1\%$, $\varepsilon_{zz} \approx -0.02\%$), a drastic decrease of the signal from the potential contacts was observed. This can be attributed to the growth of the conductivity of the central part of the sample as a result of its metallization.

The intrinsic degenerate carriers that appeared at $\sigma > \sigma_{cr}$ have made it possible to use an oscillation procedure for the investigation of the produced equal-energy surfaces. In the region $\sigma > \sigma_{cr}$, both at $\sigma\|C_2$ and at $\sigma\|C_1$, SdH oscillations were observed with a frequency that increased monotonically with increasing load (Fig. 8). In both cases the oscillations appeared only in the region $\sigma > \sigma_{cr}$ and were observed neither before application of the load nor after its removal. The
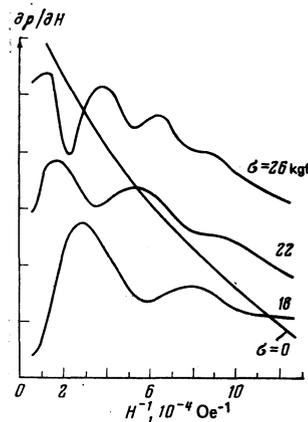
oscillation amplitude increased noticeably with increasing load.

Figure 9a shows the angular dependences of the extremal sections of the produced surface in the (C_1C_3) plane under various loads. The solid lines were drawn in accord with the ellipsoidal model. Oscillations with frequency $\approx 1.6\times10^{-42}$ (g-cm/sec)^2 from the hole surface were observed at the point T only at maximum loads $\sigma \approx 26$ kgf at angles $0-6°$ from the former direction of the C_3 axis.

It was established that neither the inclination $(6\pm0.5)°$ of the "ellipsoid" nor its anisotropy in the load interval from 18 to 26 kgf change within the limits of the experimental accuracy. According to a calculation by the McClure model with the parameters cited above for the Bi–Sb alloys, when the load is increased from 18 to 26 kgf at $\sigma\|C_2$ the Fermi energy of the elec-

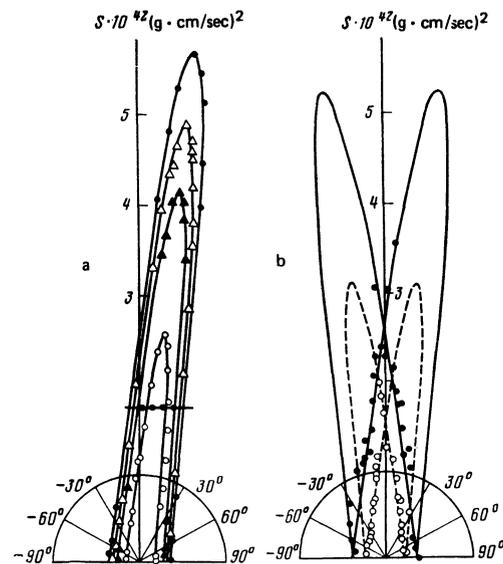FIG. 9. Angular dependences of the extremal sections of the Fermi surface produced under tension in the alloy $Bi_{0.925}Sb_{0.075}$: a—at $\sigma\|C_2$, H in the (C_1C_2) plane; b—$\sigma\|C_1$, H in the (C_2C_3) plane. Loads σ, kgf: a) $\circ$—18, $\blacktriangle$—22, $\triangle$—24, $\bullet$—26; b) $\circ$—21, $\bullet$—26. The solid and dashed lines are drawn in accordance with the ellipsoidal model.

trons at the point L_1 increases from ≈ 8 to ≈ 13 meV, while the carrier density calculated from the change of the volume of the electron ellipsoid increases in this case from $\approx 0.5 \times 10^{16}$ to 2.5×10^{16} cm^{-3}. The Fermi energy of the holes at T, under maximum loads at $\sigma \| C_2$, calculated for a quadratic dispersion law, was $\varepsilon_F^h \approx 3$ meV. Thus, the band overlap produced in this case reaches ≈ 16 meV.

At $\sigma \| C_1$, two electron equal-energy surfaces are produced (Fig. 9b). For these equal-energy surfaces $\varepsilon_{F_{2,3}}^e$ increases in the load interval $18 < \sigma < 26$ from ≈ 7.5 to ≈ 12 meV. It was impossible to separate the oscillations from the hole surface at $\sigma \| C_1$.

The semiconductor-semimetal transition was observed for the first time under uniaxial tension and differs qualitatively from the transitions of this type previously observed in the alloys $Bi_{1-x}Sb_x$ under hydrostatic compression. Namely, the transition to the metallic state was the result of the overlap of the extremum at T with one ($\sigma \| C_2$) or two ($\sigma \| C_1$) extrema in L.

PSEUDOPOTENTIAL-METHOD CALCULATION OF THE CHANGE OF THE BAND STRUCTURE OF STRAINED BISMUTH

It was indicated above that the calculation of the motion of the extrema in deformation, using a concrete model of the spectrum (for example, the McClure model) calls also for the knowledge of the dependences of the gaps ε_{gL} and ε_{gT} on the strain. Since these dependences are difficult to obtain in experiment, it is of interest to compare the obtained dtaa (see Fig. 5) with the calculation of the band structure of Bi by the pseudopotential method. In addition, these calculations can be of independent interest.

The accuracy of the calculation of the band structure by the pseudopotential method depends strongly on the assumptions made in each concrete case. The customarily employed approximations—locality of the pseudopotential, neglect of the spin-orbit interaction, confinement to the second order of perturbation theory, and others lead to an attained accuracy ≈ 0.01 Hartree (~ 0.27 eV). At the same time it is well known that the pseudopotential method is free of any fundamental limitations on the accuracy, since it is based on an exact transformation of the Schrödinger equation.

The accuracy of the calculation of the band structure can be considerably increased within the framework of an empirical pseudopotential in the presence of a large number of highly accurate experimental data on the spectrum. In the case of bismuth this became possible recently through a detailed investigation of its Fermi surface and a derivation of an empirical equation that describes the electron part of the Fermi surface with accuracy $\approx 2\%$.[33] This makes it possible to find the parameters of the pseudopotential without any other information on the band structure of bismuth. This approach differs in principle from the traditional method of fitting the pseudopotential parameters,[34] and permits calculation of the principal energy characteristics of

the bismuth spectrum with sufficient accuracy.

The form of the pseudopotential of bismuth was chosen to be the same as in Ref. 34. In the calculation of the spectrum at an arbitrary point lying on the Fermi surface, 160 plane spinor waves were taken into account exactly, while the remaining waves were taken into account in n-th order perturbation theory. The order of the perturbation theory and the number of the terms were determined from the condition that the spectra converge with accuracy not worse than 10^{-5} Hartree. From the known spectra at the points on the Fermi surface we calculated the Fermi levels ε_F^h and ε_F^e of the holes and of the electrons:

$$\varepsilon_F{}^h = \frac{1}{N} \sum_{i=1}^{N} [\varepsilon_{10}(T) - \varepsilon_{10}{}^h(x_i, y_i, z_i)], \tag{4}$$

$$\varepsilon_F{}^e = \frac{1}{N} \sum_{i=1}^{N} [\varepsilon_{12}{}^e(x_i, y_i, z_i) - \varepsilon_{12}(L)]. \tag{5}$$

Here $\varepsilon_{10}^h(x_i y_i z_i)$ is the tenth level at the point (x_i, y_i, z_i) lying on the hole Fermi surface, $\varepsilon_{12}^e(x_i, y_i, z_i)$ is the twelfth level at the point (x_i, y_i, z_i) lying on the electron Fermi surface, $\varepsilon_{10}(T)$ is the tenth level at the point T, and $\varepsilon_{12}^e(L)$ is the twelfth level at the point L. The accuracy with which the corresponding part of the Fermi surface is described was defined as the ratio of the mean squared deviation from the Fermi level to the value of this level calculated from formula (4) or (5). It was required that the initial pseudopotential describe the Fermi surface with 10% accuracy. More stringent requirements have apparently no physical meaning, since a 10% accuracy in the description of the band structure of Bi, by virtue of the smallness of the characteristic energy differences in its spectrum, is at the limit of the capabilities of the single-electron approximation of the pseudopotential: $r_0 = 0.474$, $\beta = 2.37$, $Z = 3.046$, $\lambda = 0.0125$, $A = 0.00905$. The calculated values of the Fermi energies of the electrons ε_F^e and of the holes ε_F^h of the gaps ε_{gL} and ε_{gT} at the points L and T are given in Table III. The table also indicates the most reliable, from our point of view, experimental and model-derived values of these quantities. Calculation has also shown that the level $\varepsilon_{12}(L)$ is of the L_s type, while $\varepsilon_{10}(L)$ is a level of the L_a type, confirming by the same token the inverted character of the spectrum at the point L.

In the calculation of the influence of the lattice deformation on the band structure we used a pseudopotential with the same parameters as under normal conditions, inasmuch as a crystal deformation on the order of 1% is accompanied by no noticeable deformation

TABLE III. Certain parameters* of the band structure of bismuth in the normal state.

	ε_F^e	ε_F^h	ε_{gL}	ε_{gT}
Calculation	30	15	10	237
Experiment	31±1 [25]	12 [35]	9±2 [25]	194 [35], 200±10 [25]

*Given in meV.

of the ion core. The deformation of the crystal was assumed to be equal to the deformation of the Bi sample in the rings of the type described above, averaged over the area of a circle of radius $r_1 = 0.15 r_2$. This has led to some renormalization of the matrix elements because of the change in the volume of the unit cell. The results of the calculation of the dependence of the principal sections of the electron and hole ellipsoids on the load are shown by the dashed lines of Fig. 5. The maximum discrepancy between the theoretical and experimental data occurs for the sections $S_1^e(\sigma \| C_1)$ and does not exceed 25%.

Quite interesting from our point of view are the data on the character of the change of the gaps $\varepsilon_{\varepsilon L_{1,2,3}}$ under tension. It follows from the calculation that all the gaps $\varepsilon_{\varepsilon L_{1,2,3}}$ decrease little under tension and change not more than 30% during the instant of the EPT. This result supports the assumption made in the estimates of the changes of the Bi spectrum by the McClure model, that $\varepsilon_{\varepsilon L}$ does not change with the strain. The general character of the change of the structure of the spectrum, calculated by the pseudopotential method, is shown in Fig. 5 by the dash-dot lines. The loads at which topological changes of the Fermi surface take place in the course of stretching along the binary and bisector axes are respectively 42 and 20 kgf.

The partial values of the Fermi energy for the electron ellipsoids whose volumes increase upon deformation amount at the instant of the EPT to 60 and 95 meV at $\sigma \| C_1$ and $\sigma \| C_2$, respectively, in satisfactory agreement with McClure's estimates (see Fig. 7).

CONCLUSION

As the result of the experimental and theoretical investigation of the influence of tensile strains on the spectrum of Bi and of $Bi_{1-x}Sb_x$ alloys, we obtained a general picture of the variation of the structure of the energy spectrum of the substances when strained along the principal crystallographic directions. Even though the character of the strains produced by the employed method differ somewhat from the tensile strain of the free sample, in both cases the same change of the symmetry of the lattice takes place, and therefore the general picture of the change of the spectrum should be the same apart from some numerical calculations. Therefore the character of the EPT in tension along the principal crystallographic directions should be the same in both cases, but with critical values shifted somewhat along the deformation axes. There are likewise no grounds for assuming that the change of the Fermi surface following tension of the free sample will be substantially different.

The topological transitions that make it possible to obtain rather exotic spectra for bismuth with one (or two) electron extrema, not only uncover new possibilities for obtaining more accurate information on the parameters of the spectrum (investigation of the Fermi surface made up of one ellipsoid), but also attest to the applicability, with sufficient degree of accuracy, of the theoretical spectrum models for bismuth and for the alloys[24] $Bi_{1-x}Sb_x$ to crystal structures distorted as a result of deformation.

It was indicated above that a direct measurement of the gaps $\varepsilon_{\varepsilon L}$ is a very complicated task. However, the qualitatively same character of the shifts of the identical extrema L_i for pure bismuth (inverted spectrum) and for the alloys $Bi_{1-x}Sb_x$ in the region of the direct spectrum allow us to conclude that the corresponding terms L_a and L_s are shifted in energy in the same direction with changing deformation, and the gaps $\varepsilon_{\varepsilon L}$ vary slowly, since rates of divergence of the extrema in both cases do not differ substantially. This conclusion agrees qualitatively with the results of calculation of the motion of the terms by the pseudopotential method.

---

1) Although the threefold symmetry axis vanishes upon uniaxial deformation in the basal plane, we shall use, for convenience, the direction of the former trigonal axis to define the orientation of the sample.

[1] N. B. Brandt, E. S. Itskevich, and N. Ya. Minina, Usp. Fiz. Nauk **104**, 459 (1971) [Sov. Phys. Usp. **14**, 438 (1972)].

[2] J. V. Svechkarev and A. S. Panfilov, Phys. Status Solidi **63**, 11 (1974).

[3] J. E. Shyrber, Honda Memorial Ser. on Mat. Sci., Tokyo, 1974, p. 141.

[4] J. M. Perz and R. H. Hum, Can. J. Phys. **49**, 1 (1971).

[5] M. M. Finkelstein, J. Low Temp. Phys. **14**, 287 (1974).

[6] J. J. Gerstein and C. Elbaum, Phys. Status Solidi B **57**, 157 (1973).

[7] J. de Wilde and D. J. Meredith, J. Phys. E. **9**, 62 (1976).

[8] D. Shoenberg and B. R. Watts, Philos. Mag. **15**, 1275 (1967). D. Gamble and B. R. Watts, Phys. Lett. **40A**, 22 (1972).

[9] A. J. Slavin, Philos. Mag. **27**, 65 (1972).

[10] E. Fawcett, R. Griessen, and D. J. Staley, J. Low Temp. Phys. **25**, 771 (1976). R. Griessen, D. J. G. Lee, and D. J. Stanley, Phys. Rev. B **16**, 4385 (1977). D. J. Stanley, J. M. Perz, M. J. G. Lee, and R. Criessen, Can. J. Phys. **55**, 344 (1977).

[11] P. I. Baranskiĭ, V. V. Kolomiets, and A. F. Fedosov, Fiz. Tekh. Poluprovodn. **10**, 2179 (1976) [Sov. Phys. Semicond. **10**, 1296 (1976)].

[12] N. B. Brandt, V. F. Keptya, V. A. Kul'bachinskiĭ, and N. Ya. Minina, Prib. Tekh. Éksp. No. 2, 205 (1977).

[13] N. B. Brandt, N. Ya. Minina, and V. F. Keptya, Prib. Tekh. Éksp. No. 6, 189 (1972).

[14] I. M. Lifshitz, Zh. Eksp. Teor. Fiz. **38**, 1569 (1960) [Sov. Phys. JETP **11**, 1130 (1960)].

[15] P. F. Papkovich, Teoriya uprugosti (Theory of Elasticity), Moscow, Oborongiz, 1939.

[16] J. Eckstein, A. W. Lowson, and O. H. Reneker, J. Appl. Phys. **31**, 1534 (1960).

[17] A. L. Jain and R. Jaggi, Phys. Rev. **135**, N 3A, 708 (1964). R. T. Bate, W. T. Drobish, and N. G. Einspruch, Phys. Rev. **149**, 485 (1966).

[18] M. E. Ertl and J. U. Rahman, Phys. Status Solidi B **45**, 85 (1971). F. J. Bekkerman and D. V. Gitsu, Phys. Status Solidi B **74**, K1 (1976).

[19] N. B. Brandt and G. A. Ryabenko, Zh. Eksp. Teor. Fiz. **37**, 389 (1959) [Sov. Phys. JETP **10**, 278 (1960)]. R. T. Bate and N. G. Einspruch, Phys. Lett. **16**, 11 (1965).

[20] P. R. Aron and N. G. Chandrasekhar, Phys. Lett. **30A**, 86 (1969).

[21] Yu. P. Gaĭdukov, N. P. Danilova, and M. B. Shcherbina-Samoĭlova, Fiz. Nizk. Temp. **4**, 250 (1978) [Sov. J. Low Temp. Phys. **4**, 124 (1978)].

[22] N. B. Brandt, V. A. Kul'bachinskiĭ, and N. Ya. Minina, Fiz. Tverd. Tela (Leningrad) **18**, 1829 (1976) [Sov. Phys. Solid State **18**, 1065 (1976)].

570   Sov. Phys. JETP 51(3), March 1980

Brandt et al.   570

[23]N. B. Brandt, V. A. Kul'bachinskiĭ, and N. Ya. Minina, Pis'ma Zh. Eksp. Teor. Fiz. **26**, 173 (1977) [JETP Lett. **26**, 166 (1977)].

[24]J. W. McClure, J. Low Temp. Phys. **25**, Nos. 5/6, 527 (1976).

[25]R. Myuller, Abstract of Candidate's Dissertation, Moscow State Univ., 1979.

[26]N. B. Brandt and Ya. G. Ponomarev, Proc. 10th Internat. Conf. on Low Temp. Phys., Vol. 3, VINITI, p. 310; Zh. Eksp. Teor. Fiz. **55**, 1215 (1968) [Sov. Phys. JETP **28**, 635 (1969)].

[27]E. S. Itskevich and A. N. Voronovskiĭ, Pis'ma Zh. Eksp. Teor. Fiz. **4**, 226 (1966) [JETP Lett. **4**, 154 (1966)].

[28]N. B. Brandt, N. I. Ginzburg, T. A. Ignat'eva, B. G. Lazarev, A. S. Lazareva, and V. I. Makarov, Zh. Eksp. Teor. Fiz. **48**, 7 (1965) [Sov. Phys. JETP **21**, 4 (1965)].

[29]N. B. Brandt, V. A. Kul'bachinskiĭ, and N. Ya. Minina, Fiz.

Nizk. Temp. **4**, 527 (1978) [Sov. J. Low Temp. Phys. **4**, 258 (1978)].

[30]N. B. Brandt, V. A. Kul'bachinskiĭ, and N. Ya. Minina, Pis'ma Zh. Eksp. Teor. Fiz. **26**, 637 (1977) [JETP Lett. **26**, 484 (1977)].

[31]E. P. Buyanova, V. V. Evseev, G. A. Ivanov, G. A. Mironova, and Ya. G. Ponomarev, Fiz. Tverd. Tela (Leningrad) **20**, 1937 (1978) [Sov. Phys. Solid State **20**, 1119 (1978)].

[32]N. B. Brandt, S. M. Chudinov, and V. G. Karavaev, Zh. Eksp. Teor. Fiz. **70**, 229 (1976) [Sov. Phys. JETP **43**, 1198 (1976)].

[33]V. S. Édel'man, Zh. Eksp. Teor. Fiz. **64**, 1734 (1973) [Sov. Phys. JETP **37**, 875 (1973)].

[34]S. Golin, Phys. Rev. **166**, 643 (1968).

[35]M. S. Dresselhaus, Phys. Rev. B **14**, 1370 (1976).

Translated by J. G. Adashko

Isostructural instability and physical properties of the Hubbard long-range model

R. O. Zaĭtsev

I. V. Kurchatov Atomic Energy Institute
(Submitted 31 July 1979)
Zh. Eksp. Teor. Fiz. **78**, 1132–1146 (March 1980)

The use of the large-number-of-nearest-neighbor approximation enables us to evaluate the polarization operator which defines the permittivity and the phonon spectrum renormalization. We evaluate the long-range correction to the free energy in the vicinity of the metal-dielectric transition (*M*- or Mott-transition). We show that in the region of strong correlations the system loses its mechanical stability so that the *M*-transition is accompanied by a first-order isostructural transition. Far from the transition and for sufficiently low temperatures the singularities of the thermodynamic quantities are weakened and remind us of those near a second-order transition.

INTRODUCTION

In the theory of structural transformations which accompany the transition from the metallic to the dielectric state one uses in an essential way the assumption that the electron-electron interaction is small. For instance, in the theory of an exciton dielectric[1,2] all calculations of the irreducible vertex part are restricted to the second order of perturbation theory. In Adler's theory[3] one assumes that the cause of the structural transition is the strong electron-phonon interaction. The direct electron-electron interaction does not occur at all in this theory. In the Hubbard model[4] the strong interaction of the electrons (u) is taken into account right from the beginning. One can therefore expect that a correct allowance for the electron-phonon and electron-electron interactions (in different cells) in that model will lead us appreciably closer to an understanding of the physical effects which take place in the oxides, sulfides, and nitrides of transition metals.

We assume that the energy for the transition to a neighboring cell (t) is smaller than the energy of the electron interaction in one and the same cell (u). One

can then easily show[5] that in the Hubbard model there occurs a structural transition if the electron-phonon interaction energy reaches a value of the order of u. Such a situation may be an exception—as a rule the opposite situation occurs. The electron-phonon interaction is equivalent to an attraction which is of the same order of magnitude as (or less than) the Coulomb interaction between different cells which, in turn, is less than the energy u. Because of this we shall neglect in the present paper the ion motion, assuming that its role reduces to providing electro-neutrality on the whole. Taking the long-range part of the Coulomb interaction into account makes our model close to the well known Shubin-Vonsovskii model[6] where the problem was posed of finding the ground state of a system with an arbitrary interaction between different cells.

We shall consider in the present paper the first-order isostructural transition which accompanies the Mott transition. We shall show that the rearrangement of the electron spectrum near the *M*-transition line strongly changes the long-range part of the Coulomb interaction. The permittivity increases in the dielectric phase when the pressure increases and becomes infinite at the Mott